

# Formulation and validation of Candesartan cilexetil-loaded nanosuspension to enhance solubility

Sarmad Al-Edresi<sup>1</sup>, Karrar Albo Hamrah<sup>1</sup>, Abulfadhel Al-Shaibani<sup>1</sup>

<sup>1</sup> Department of Pharmaceutics and Industrial Pharmacy, University of Kufa, Najaf 52001, Iraq

Corresponding author: Sarmad Al-Edresi (s.aledresi@uokufa.edu.iq)

Received 30 October 2023 ♦ Accepted 28 February 2024 ♦ Published 19 March 2024

**Citation:** Al-Edresi S, Albo Hamrah K, Al-Shaibani A (2024) Formulation and validation of Candesartan cilexetil-loaded nanosuspension to enhance solubility. *Pharmacia* 71: 1–13. <https://doi.org/10.3897/pharmacia.71.e114943>

## Abstract

The following research aimed to enhance solubility by loading candesartan cilexetil into nanosuspension. Candesartan cilexetil-loaded nanosuspension was prepared with the aid of Design-Expert® software. A technique of solvent evaporation was employed to produce nanosuspensions from hydroxyl propyl methyl cellulose (HPMC E5), polyvinyl pyrrolidone (PVP K-30), and poloxamer (PXM 188). The optimised nanosuspensions' particle size and polydispersity index (PDI) were 64.65 nm and 0.059, respectively. The entrapment efficacy (EE %) and drug loading (DL %) were 86.75 and 10.17%, respectively. The atomic force microscopy (AFM) revealed spherical and smooth nanoparticles. The Fourier transform infrared spectroscopy (FTIR) and differential scanning calorimetry (DSC) revealed pure, crystalline and conjugated drugs inside the nanosuspension. The release study confirmed 90% release within 10 min. No significant changes in particle sizes over three months were found, indicating stable nanoparticles. Saturated solubility of the candesartan cilexetil powder and loaded nanosuspension was  $63.3 \pm 6$  and  $344.7 \pm 16 \mu\text{g}\cdot\text{ml}^{-1}$ , respectively, revealing more than five times increase in solubility. Candesartan cilexetil-loaded nanosuspensions were successfully prepared using different combinations of PVP K-30, HPMC E-5 and PXM 188 in various concentrations. Solubility was enhanced by loading the payload into nanosuspensions.

## Keywords

Nanosuspensions, Candesartan cilexetil, Design-Expert® software

## Introduction

Drug solubility in aqueous media is an important consideration to address early in the drug discovery process. Approximately 40% of novel chemical entities generated in the pharmaceutical sector are nearly water-insoluble (Chen et al. 2014). The biopharmaceutics classification system divides drugs into four categories: class I (very soluble and permeable), class II (highly permeable but poorly soluble), class III (highly soluble but weakly permeable), and class

IV (poorly soluble and poorly permeable) (Bonthagarala et al. 2015). High molecular weights, significant log P values and poor water solubility typically characterise the II and IV classes. Candesartan cilexetil is a prodrug that selectively antagonises the receptor of angiotensin II. After absorption from GIT, it is converted to active candesartan moiety. According to BCS, Candesartan cilexetil belongs to class II (Figueroa-Campos et al. 2020).

When a drug molecule has several limitations, such as the inability to form salt, high molecular weight, dose, log

P and melting point, nanosuspension is the only choice accessible (Bhakay et al. 2018). The inherent nature of molecular complexation employing cyclodextrin in pharmaceutical formulations to increase the formulation volume due to the considerable molecular weight of the complexing agent is a fundamental restriction. Nanosuspensions can tackle such unique drug delivery difficulties by keeping active pharmaceutical ingredients in a crystalline condition while allowing for increased DL% during formulation development. Because of the reduced usage of toxic, non-aqueous solvents and extreme pH, accommodating large amounts with minimal dose volume provides significant benefits in parenteral and ophthalmic drug delivery systems. Other benefits include enhanced stability, extended drug release, increased efficacy through tissue targeting, minimal first-pass metabolism and deep lung deposits (Kumar et al. 2020). These benefits have accelerated the development of nanosuspension technology in recent decades. Despite the difficulties of production, choosing the proper unit operation, equipment, and process optimisation can help mitigate these issues (Jacob and Nair 2018).

Pharmaceutical nanosuspensions are aqueous dispersions of insoluble drug particles that are nanosized and stabilised by surfactants (Aledresi et al. 2020). On the other hand, nanoparticles are drug carriers that are either polymeric or lipid colloidal (Edis et al. 2021). It has been reported that nanosuspensions are a universal approach to enhancing solubility for compounds insoluble in aqueous media (Jia et al. 2002). Better understanding and advances in nanosuspension technology enhance formulation development towards the fabrication of such systems. Scientists have reported the ability of nanosuspensions to increase the solubility of their payload, leading to an enhanced dissolution rate (Müller et al. 2001; Gigliobianco et al. 2018). Nanosuspensions could be prepared using a single or a combination of polymers. Using a single polymer to produce nanosuspensions was not recommended because of higher degradation rates and lower mechanical properties (Adeli et al. 2019). Many researchers have suggested using polymer combinations in producing nanosuspensions as they have good physical properties and produce homogeneous nanosuspensions (Wilk and Benko 2021). Many researchers nominated a vast number of polymers to prepare nanosuspensions. However, PVP, HPMC and PXM were mainly selected for the following reasons. The PVP is a synthetic polymer with good chemical, optical, thermal and electrical stabilities, biocompatibility, biodegradability, biosafety and improved physical and mechanical properties (Demirci et al. 2009; Wang et al. 2012; Archana et al. 2015). The HPMC has good water solubility with low mechanical properties; therefore, it is recommended to be mixed with natural or synthetic polymers (Balogh et al. 2016; Aydogdu et al. 2019). PXM was recognised by The Food and Drug Administration (FDA) as a pharmaceutical excipient. Because of its commercial availability, safety and versatility, it is often used as a nanocarrier (Zhang et al. 2015). PXM was reported

as a good nominant to enhance the permeation of drugs and absorption, using its excellent properties to improve aqueous solubility (Li et al. 2020).

Candesartan cilexetil-loaded nanosuspensions have been fabricated by Dabhi and his colleague (2015) (Dabhi et al. 2015) using high-speed homogenisation and media milling and reported a particle size of < 500 nm and enhanced solubility. Aly et al., (2020) (Aly et al. 2020) prepared Candesartan cilexetil-loaded nanosuspension using different techniques to improve the bioavailability of candesartan cilexetil. They produced stable nanoparticles using the antisolvent method for PVP K90, whereas the bioavailability increased from 15% to 48%. The following research aimed to enhance the solubility of candesartan cilexetil by loading it into nanosuspension from a combination of polymers with the aid of Design-Expert® software.

## Materials and methods

### Material

Candesartan cilexetil powder was purchased from Wuxi Hexia Chemical Company, Chin. HPMC E5 and PXM-188 were purchased from Hyperchem (China). Disodium hydrogen phosphate ( $\text{Na}_2\text{HPO}_4$ ) was purchased from CDH (India). Potassium dihydrogen phosphate ( $\text{KH}_2\text{PO}_4$ ) was purchased from Himdia (India). Sodium chloride ( $\text{NaCl}$ ) was purchased from LAD (India). The PVP K-30 was purchased from Alpha Chemika (India), and ethanol was purchased from HaymanKimia (U.K.).

### Method

#### *Factorial design to optimise the formulation*

A Full factorial design for three factors (stabilisers' concentrations) at three levels was selected to optimise the variables' response (particle size, PDI, EE% and DL%). Appropriate HPMC E5, PVP K-30 and PXM 188 concentrations needed to create a nanosuspension were determined with the best possible responses. Independent variables were the concentrations of A (PVP K-30), B (HPMC E5) and C (PXM 188). However, the dependent variables were  $R_1$  (particle size),  $R_2$  (PDI),  $R_3$  (EE%), and  $R_4$  (DL%), which were taken as the response variables. In this design, three factors at three levels of concentrations were assessed: lower (25 mg), middle (112.5 mg) and higher (200 mg). The factors with the corresponding codes representing -1, 0 and +1 were employed in this design and trials of the experiments for all possible combinations were performed. As a result, eighteen proposed runs were produced to cover the entire area of experiments listed in Table 1. Some runs in the same concentrations were replicated by Design-Expert® software to estimate the lack of fit and detect any possible hand errors. Other formulation processing variables were kept constant in the study.

**Table 1.** The 2<sup>3</sup> factorial design of candesartan cilexetil-loaded nanosuspension.

Run	PVP K-30 (A)	HPMC E5 (B)	PXM 188 (C)
1	-1	1	1
2	-1	-1	-1
3	1	-1	-1
4	1	-1	1
5	0	0	0
6	1	-1	1
7	1	1	-1
8	-1	-1	1
9	-1	-1	-1
10	1	1	1
11	-1	-1	1
12	0	0	0
13	1	1	1
14	-1	1	1
15	-1	1	-1
16	-1	1	-1
17	1	1	-1
18	1	-1	-1

The effect of the independent variables on the response was analysed. The response regression equation was calculated using Equation 1.

Response:

$$Y = b_0 + b_1A + b_2B + b_3C + b_4AB + b_5AC + b_6BC + b_7ABC \quad \text{E.q. 1}$$

Where: Y is the quantitative effect of the independent variables, while b is the coefficient of the independent variables (A, B and C). Changing one factor at a time (average results) represents the main effect (A, B and C) from its low to high value. Changing responses when two factors are simultaneously changed were shown by the interaction term (ABC).

## Data analysis and desirability function

The current optimisation study used various response surface methodology (RSM) computations using Design-Expert<sup>®</sup> software (Version 13, Stat-Ease Inc., Minneapolis, MN). Three factorial designs of the factorial models were generated for all responses. Also, 3D plots were constructed using Design-Expert<sup>®</sup> software. Analysis of variance (ANOVA, 2-way) was used to assess the significance of the selected parameters on the variables. The desirability function was employed after fitting the mathematical model for the optimisation. During the optimisation process, the responses were combined to find a product with high desirability. The desirability function combined all responses into one variable to predict the optimum levels gained from the independent variables. A desirability value ranged from zero to one. Thus, zero is an unacceptable value for the responses, while one is the most desired value. The selected optimised formulation by the design was prepared, and a comparison was carried out between predicted and observed values given by the design.

## Preparation of Candesartan cilexetil-loaded nanosuspension

Candesartan cilexetil nanosuspensions were prepared using the solvent evaporation technique. The candesartan cilexetil powder, 6 mg, was dissolved in 2 ml of ethanol (solvent) to create the drug solution. The candesartan cilexetil solution was injected at a rate of 1 ml.min<sup>-1</sup> into 20 ml of distilled water (anti-solvent). The stabilisers were solubilised in distilled water 5 min pre-injections and involved combinations in various concentrations (A, B and C). Next, the prepared nanosuspensions were exposed to sonication for 20 min in a water bath. As a result, nanoparticles started to form simultaneously. A one-hour magnetic stirrer homogenised the produced nanosuspensions and evaporated the organic solvent. Ultimately, a lyophilised Labconco freeze drier (USA) has been employed to remove any traces of solvent.

## Determination of melting point

The method of determining the melting point of candesartan cilexetil was adapted from Karar et al. (2020) (Albo Hamrah et al. 2020). A small amount of candesartan cilexetil powdered was mounted into a capillary glass tube. The glass tube was opened from one side and closed from the other. The temperature inside the glass tube was gradually raised and inspected visually. The temperature was recorded when the solid powder melted completely. This analysis would be replicated three times independently to obtain mean ± standard deviations.

## Determination of the maximum λmax of candesartan cilexetil

The maximum λmax of candesartan cilexetil was determined according to our previous published work (Albo Hamrah et al. 2020). Stock solutions of candesartan cilexetil were prepared in HCl buffer (pH 1.2) and phosphate buffer (pH 6.8) at a concentration of 30 µg per ml. The range of UV-visible was 200–400 nm; hence, these solutions were scanned using a UV-visible instrument (Shimadzu, Japan). This analysis would be replicated three times independently so that mean ± S.D. would be obtained.

## Construction calibration curves of candesartan cilexetil

The method of construction of a calibration curve for the quantification of candesartan cilexetil was obtained from our previous published work (Albo Hamrah et al. 2020). This method was based on preparing a stock solution from dissolving candesartan cilexetil in HCl buffer (pH 1.2) and phosphate buffer pH (6.8) at 50 µg per ml. Next, serial dilutions of 5, 10, 20, 30 and 50 concentrations were prepared. Spectrophotometrically, these solutions were analysed at λmax 254 nm and plotted against concentrations

to get the calibration curve. The calibration curve was ultimately constructed to gain the calibration curve equation and regression coefficient (R<sup>2</sup>) value. This analysis would be replicated three times independently so that mean  $\pm$  S.D. would be obtained.

### **Saturated solubility of candesartan cilexetil**

The method of determining the saturated solubility of candesartan cilexetil was based on our previous published work (Albo Hamrah et al. 2020). An excess candesartan cilexetil powder was added to a 10 ml tube containing 5 ml HCl buffer (pH 1.2). Next, these tubes were shaken at  $25 \pm 0.5$  °C in an isothermal shaking water bath for 72 h. Then, they were centrifugated for 10 min at 2000 rpm (R LABNCO, USA) to remove the supernatant. The supernatants were filtered using a filter membrane (0.45  $\mu$ m) and scanned at maximum absorption wavelength using a UV-visible spectrophotometer (Shimadzu, Japan).

### **Particle size and polydispersity index analysis**

Particle size parameters were determined using the ABT-9000 Nano Laser particle size analyser at a constant temperature of 25 °C and a scattering angle of 90°. The prepared nanosuspensions' R1 (particle size) and R2 (PDI) were measured. The sample with a low polydispersity index means monodisperse, while a high level means wide-spread particle distribution. The average level of PDI values is 0–0.05, which means monodisperse standard, 0.05–0.08 refers to nearly monodisperse, 0.08–0.7 indicates mid-range PDI and more than 0.7 means very polydisperse (Satyajit et al. 2014; Alhagies and Gharreb 2021).

### **Determination of entrapment efficiency (EE%) of candesartan cilexetil**

The method used to determine EE% was based on the work of Hao (2011) with minor modifications (Hao 2011). The sample (1 mg) was placed in the dialysis membrane and dialysed in 100 ml of phosphate buffer (pH 6.5) for 12 h. Then, the entrapped candesartan cilexetil in the dialysis membrane was quantified. The EE% was measured by dividing the trapped amount by the total used amount (Abdalla et al. 2015; Huang et al. 2020).

### **Development and evaluation of the optimised formulation**

Among nine runs, the Design-Expert<sup>®</sup> software has developed an optimal formula based on maximising EE% and minimising particle size and polydispersity index. A desirable index was generated and compared with the resulting suggestions, with a value between 0 and 1. These criteria were established, and the best formula was chosen (Madan et al. 2015).

## **Freeze drying of nanosuspension**

Samples of Candesartan cilexetil-loaded nanosuspensions were solidified by lyophilisation technique by water removal. This technique used the principle of sublimation and desorption with a negative vacuum (Powar and Hajar 2020). Nanosuspensions were frozen at -30 °C for 12 h and then lyophilised using a freeze dryer (Christ, Osterode, Germany). The operating conditions of the freeze dryer were a pressure of 20 mbar and a temperature of -50 °C (Fonte et al. 2016).

### **Morphological studies using AFM analysis**

Morphological analysis using AFM is a powerful tool to investigate surfaces of samples. It provides high-resolution images to examine nanoparticles precisely. Histograms of particle size distribution, particle size, and 3D surface morphology of Candesartan cilexetil-loaded nanosuspensions were obtained (Dolenc et al. 2010).

A mica disc was mounted on a metal base, and 10  $\mu$ l of nanosuspensions were deposited on the mica disc (Al-Edresi et al. 2020). Samples were washed five times using filter-sterilised Milli-Q water and then air dried at room temperature. Furthermore, images were taken using a Picoforce Nanoscope V Multimode atomic force microscope (Bruker). The mode was tapping, the scanning rate was between 0.5 and 1.5 Hz, and the resonant frequency range was 270–460 kHz. Representative areas were first specified, and then images were captured. The amplitude error mode (5 mm  $\times$  5 mm) and the height were determined using Nanoscope software v7.2 after flattening, while the determined resolution of the images was 512  $\times$  512 points.

### **Compatibility analysis using DSC analysis**

The compatibility of candesartan cilexetil and other additives in the nanosuspensions was analysed by DSC. The crystal state of the model drug, particularly when incorporated into nanosuspension, was significant (Jassim and Hussein 2014). The thermal characteristics of the pure candesartan cilexetil, A (PVP K30), B (HPMC E5), and C (PXM 188) were examined by an automatic thermal analyser system (Perkin-Elmer DSC 4000) instrument (Rizal et al. 2020). The thermograms of the control (candesartan cilexetil free) nanosuspensions and candesartan cilexetil-loaded nanosuspensions were recorded. Nanosuspensions were first frozen and lyophilised using a freeze-dryer (Martin Christ alpha 1–4 L.D. 92 plus, Germany) at 0.01 bar and -55 °C. Then, 5 mg was sealed by crimping an aluminium lid in an aluminium pan with a crimper press (Perkin-Elmer, U.K.). Next, the temperature of the DSC was raised from 0 °C to 280 °C at a scan rate of 10 °C  $\cdot$  min<sup>-1</sup>. The used reference was an empty pan with a lid. The plots were generated by StarE 9.10 software (Isailović et al. 2013).

## Drug-excipient compatibility studies using FTIR

The FTIR analysis was carried out to gain spectra of the Candesartan cilexetil-loaded nanosuspensions, nanosuspensions-free candesartan cilexetil, pure candesartan cilexetil, A (PVP K30), B (HPMC E5), C (PXM 188). Samples were mixed with crushed potassium bromide and compressed into a thin tablet. The range of the resulting spectra was from 4000 to 400  $\text{cm}^{-1}$  with a resolution of 2  $\text{cm}^{-1}$  and was gained using a Nicolet Avatar 370 instrument (Thermo Nicolet Corporation, USA) (Ahmed and Aljaeid 2017).

## In vitro release study

A study of the *in vitro* candesartan cilexetil release was adapted from Jigar Shah and his colleagues (2020) with minor modifications (Shah et al. 2020). A modified Franz diffusion cell, which has a receptor and donor compartment separated by a membrane, has been used. The receptor volume was 15 ml, and the diffusion area was 1.4  $\text{cm}^2$ . The cut-off of the dialysis membrane was 8000–14000 (Sigma- Aldrich Corp. St. Louis, MO, USA). The membrane was soaked in phosphate buffer (pH 6.8) for 24 hours before use. On one face, the dialysis membrane was in contact with the receptor medium, composed of phosphate buffer (pH 6.8). The other face of the membrane contains samples having candesartan cilexetil. Both compartments' temperatures were kept constant at  $37 \pm 2^\circ\text{C}$  by submerging them in the water bath. The same experiment was repeated for HCl buffer (pH 1.2). Homogenisation inside the receptor compartment was maintained throughout the experiment using a magnetic stirrer bar rotated at 100 rpm using a hot plate magnetic stirrer (aLFA, china). A 0.5 ml sample was withdrawn at predetermined intervals for one hour and immediately replaced with fresh phosphate buffer (pH 6.8). The withdrawn samples were assayed spectrophotometrically (Shimadzu, Japan) at 254.

## Stability study

The stability study was conducted according to the guidelines of ICH. The Candesartan cilexetil-loaded nanosuspensions were exposed to three different temperatures, which were  $32 \pm 2^\circ\text{C}$  (high),  $25 \pm 2^\circ\text{C}$  (average) and  $4 \pm 2^\circ\text{C}$  (low). Samples were analysed (quantification of payload drug) monthly for three months to measure particle size and EE % (Sambhakar et al. 2017; Mittal et al. 2020).

## Statistical analysis

The t-test and ANOVA were conducted using IBM SPSS version 20 and Design-Expert® software version 9. A significant p-value was obtained at  $\leq 0.05$ . Standard deviations and means were measured by Microsoft Excel 2020, and data are expressed as mean  $\pm$  standard deviation. Where necessary, data were normalised to percentages. Comparisons are always made according to a control condition.

## Results and discussion

### Melting point of candesartan cilexetil

The recorded melting point of candesartan cilexetil was  $171^\circ\text{C}$  to  $172^\circ\text{C}$ . Results from the following experiment were consistent with the finding of Al-Shaibani and his colleagues (2019), who indicated that the pure powder of candesartan cilexetil would melt at  $171\text{--}172^\circ\text{C}$  (Al-Shaibani et al. 2019).

### Maximum $\lambda_{\text{max}}$ of drug candesartan cilexetil

It has been found that the maximum  $\lambda_{\text{max}}$  for candesartan cilexetil in phosphate buffer (pH 6.8) and HCl buffer (pH 1.2) appeared at 254 nm. Results from this experiment were consistent with the findings published by Pradhan and his colleagues (2011) (Pradhan et al. 2011).

### Calibration curves of candesartan cilexetil in (pH 1.2) and (pH 6.8)

Two calibration curves were constructed at pH 1.2 and 6.8 with regression coefficients of 0.9991 and 0.9998, respectively. Absorbencies against concentrations were taken, and a straight line was drawn using Excel software. The generated curves from the selected concentrations agreed with Beer-Lambert's law at  $\lambda_{\text{max}}$  254 nm, as shown in Figs 1, 2.

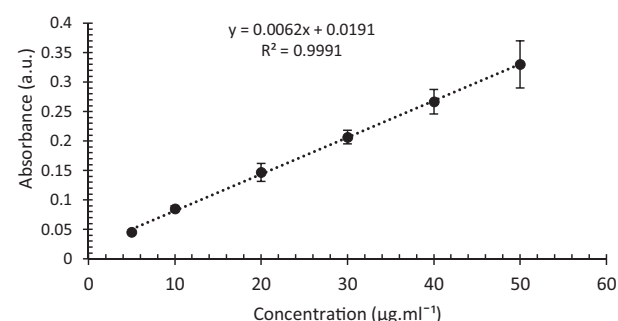


**Figure 1.** Calibration curve of candesartan cilexetil in HCl buffer (pH 1.2). Candesartan cilexetil was dissolved in HCl buffer (pH 1.2) at a concentration of 5, 10, 20, 30 and 50  $\mu\text{g.ml}^{-1}$ , and the U.V. absorbance at  $\lambda_{\text{max}}$  254 nm was gained. Data are represented as mean  $\pm$  standard deviation of 3 independent experiments.

### Saturated solubility of candesartan cilexetil

Results revealed that the saturated solubility of candesartan cilexetil was  $63 \pm 6 \mu\text{g.ml}^{-1}$  in phosphate buffer at pH 6.8 and  $7 \pm 0.35 \mu\text{g.ml}^{-1}$  in HCl buffer at pH 1.2. Hoppe, K. and M. Sznitowska (2014) have presented similar findings (Hoppe and Sznitowska 2014). It has been suggested that candesartan cilexetil has weak acidic properties as its solubility was higher in primary mediums (Ardiana et al. 2012). The saturated solubility of the candesartan cilexetil-loaded nanosuspension was  $344.7 \pm 16 \mu\text{g.ml}^{-1}$ ,

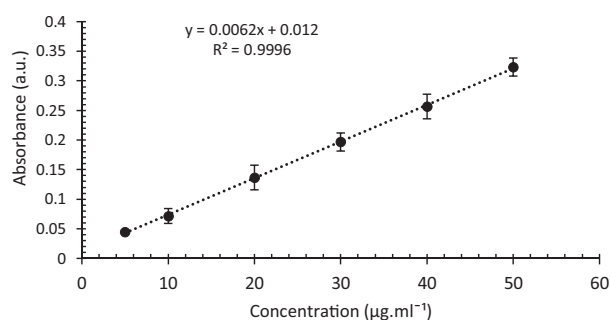


**Figure 2.** Calibration curve of candesartan cilexetil in phosphate buffer (pH 6.8). Candesartan cilexetil was dissolved in phosphate buffer (pH 6.8) at a concentration of 5, 10, 20, 30 and 50  $\mu\text{g}\cdot\text{ml}^{-1}$ , and the U.V. absorbance at  $\lambda_{\text{max}}$  254 nm was gained. Data are represented as mean  $\pm$  standard deviation of 3 independent experiments.

revealing a more than five times increase in solubility than phosphate buffer (pH 6.8) and a 9-time increase in solubility than HCl buffer (pH 1.2). The results of the increase in solubility of candesartan cilexetil-loaded nanosuspension were consistent with the findings of Detroja et al. (Detroja et al. 2011), who reported a 20 times increase in solubility through loading candesartan cilexetil into nanosuspension.

### Particle size, PDI, EE% and DL% analysis

The results of the particle size ranged from 15.6 to 155 nm. The variations in the particle sizes could be attributed to the polymer concentrations and affinities of molecules for drug particles (Liu et al. 2015). The largest particle size was revealed in Run 12 (155 nm), while the smallest was realised in Run 18 (15.6 nm), as illustrated in Table 2. The variation in particle size might be due to the high percentage of stabilisers. An increased stabiliser ratio would reduce surface tension, stabilising the new particles during precipitation. As a result, smaller particle sizes would be generated as stabilisers would wrap the surface of the particles properly. Bernard and his colleagues have come up with similar findings (Van Eerdenbrugh et al. 2009), as he reported that increasing stabilisers would decrease particle size.

The PDI ranged from 0 to 0.12 for runs 5 and 12, respectively (Table 2). Run 9 revealed a monodispersed PDI, while Run 17 revealed a mid-range PDI (Gadad et al. 2012; Abbas et al. 2017).

Results of the EE% of candesartan cilexetil in nanosuspension revealed 91.9% in Run 11, which was the highest EE%. On the contrary, Run 1 has only 51.6%, as listed in Table 2. Such variations in the EE% could be attributed to the differences in the concentration of HPMC E5; hence, increasing HPMC concentration would decrease EE% because of the increased viscosity of the internal phase. The highly viscous internal phases hindered the migration of its payload, resulting in reduced EE% (Sharma et al. 2015).

**Table 2.** The  $2^3$  factorial design responses parameters of Candesartan cilexetil-loaded nanosuspensions' formulations.

Run	Particle size (nm) (R1)	PDI (R <sub>2</sub> )	EE% (R <sub>3</sub> )	DL% (R <sub>4</sub> )
1	19.2	0.024	51.6	5.37
2	104	0.05	90.8	9.56
3	39.2	0.06	74.3	5.72
4	194	0.09	48.4	8.07
5	13.2	0.00	76.8	5.91
6	31.7	0.029	61.5	7.94
7	12.4	0.011	95.7	15.95
8	102	0.114	65.9	10.98
9	19.8	0.01	87.6	11.30
10	44.3	0.055	90.5	9.53
11	107.1	0.045	91.9	36.76
12	155	0.120	80.2	13.37
13	115	0.055	55.9	9.32
14	19.9	0.015	57.8	9.63
15	118.8	0.032	57.6	6.06
16	49.3	0.046	63.5	6.68
17	145.6	0.058	91.5	36.62
18	15.6	0.010	78.7	8.28

Results of the DL% ranged from 5.37% (Run 1) to 36.76% (Run 11) as listed in Table 2. The DL% was shown to increase as polymer concentrations increased, and this result was consistent with the finding of Dora and his colleagues (2010), who found that an increase in the polymer ratio and EE % increased the DL % (Dora et al. 2010).

### Experimental design and analysis

The Design-Expert<sup>®</sup> software and fit statistics analysed the resulting data listed in Table 3. Parameters were generated, such as predicted determination coefficient (pred. R<sup>2</sup>), p-value, adjusted determination coefficient (adj. R<sup>2</sup>) and ANOVA for all responses. A p-value of (ABC) was 0.785, 0.843, 0.037 (i.e.,  $\leq 0.05$ ) and 0.172 for R<sub>1</sub>, R<sub>2</sub>, R<sub>3</sub> and R<sub>4</sub>, respectively. This indicates that only the R<sub>3</sub> model was significant. Thus, the three polymers have a significant effect on this response.

**Table 3.** Fit statistics of the responses generated by Design-Expert<sup>®</sup> software.

Parameters	Particle size	PDI	EE%	DL%
<b>Standard deviation</b>	64.145	0.0405	10.997	8.082
<b>Mean</b>	72.561	0.0458	73.344	12.058
<b>C.V. %</b>	88.401	88.39	14.994	67.023
<b>R<sup>2</sup></b>	0.2753	0.262	0.740	0.603
<b>Adj. R<sup>2</sup></b>	-0.232	-0.312	0.538	0.294
<b>Pred. R<sup>2</sup></b>	-1.316*	-1.952*	-0.040*	-0.589*
<b>Adeq. Precision</b>	2.182	2.097	5.003	3.485
<b>p-value</b>	0.784	0.843	0.037	0.173

\* A negative Pred. R<sup>2</sup> implies that the overall mean may better predict the response.

Factorial design for three factors at three levels coded as -1, 0 and +1 was equivalent to an 18 run and was chosen as the experimental design. This is considered an

effective first-order design with a minimum number of experiments. Thus, the influence of individual variables was estimated to be the main effect. Besides, the response surface was determined, adding additional advantages to this design. Therefore, a full factorial design was employed to investigate the factors systematically.

The effect on particle size ( $R_1$ ) was observed to be non-significant by ANOVA, as shown in Equation 2.

$$R_1 = 72.56111 + 3.60625A - 5.55625B + 8.03125C + 10.15625AB + 13.49375AC - 23.99BC + 2.79375ABC \quad \text{E.q. 2}$$

The negative sign shown in Equation 2 related to the coefficient of factor B (HPMC) indicates that the particle size decreases as the concentration of B increases. The findings from this analysis agreed with the findings from Mandlik and Ranpise (2017) (Mandlik and Ranpise 2017), who reported that chitosan concentration on nanoparticle size was more pronounced than STPP. The response surface 3D plots revealed that the particle size headed toward the upper level at low concentrations, as shown in Fig. 3a. The reduction in the particle size resulted from increasing HPMC concentrations due to supersaturation, which led to rapid precipitation during diffusion (Sahu and Das 2013). Agglomeration or aggregation might be induced on a smaller concentration of the stabiliser; however, adding stabiliser in too much concentration could promote Oswald's ripening (Tadros 2017).

The effect on PDI ( $R_2$ ) was observed to be non-significant by ANOVA, as shown in Equation 3.

$$R_2 = 0.0440 + 0.0020A - 0.0070B + 0.0094C + 0.0058AB + 0.0019AC - 0.0091BC + 0.0081ABC \quad \text{E.q. 3}$$

The PDI, which reflects the uniformity of size, was more dependent on stabiliser concentration. Results indicated that PDI decreases as the stabiliser concentration increases, as shown by the negative charge in Equation 3. As PDI decreased, better homogeneity was gained; however, less homogeneous particles were obtained at very high stabiliser concentrations. The response surface 3D plots revealed that the PDI is heading toward the upper level at low concentrations, as shown in Fig. 3b.

The effect on EE% ( $R_3$ ) was observed to be significant by ANOVA, as shown in Equation 4.

$$R_3 = 72.70 + 1.86A - 2.19B - 7.26C + 11.03AB - 3.23AC + 0.7000BC - 0.4125ABC \quad \text{E.q. 4}$$

A stabiliser A revealed a positive sign for the coefficient, indicating that the EE% increases as the stabiliser concentration increases. The response surface 3D plots (Fig. 3c) showed a linear ascending pattern for EE% with increasing stabiliser concentration.

The effect on DL% ( $R_4$ ) was observed to be non-significant by ANOVA, as shown in Equation 4.

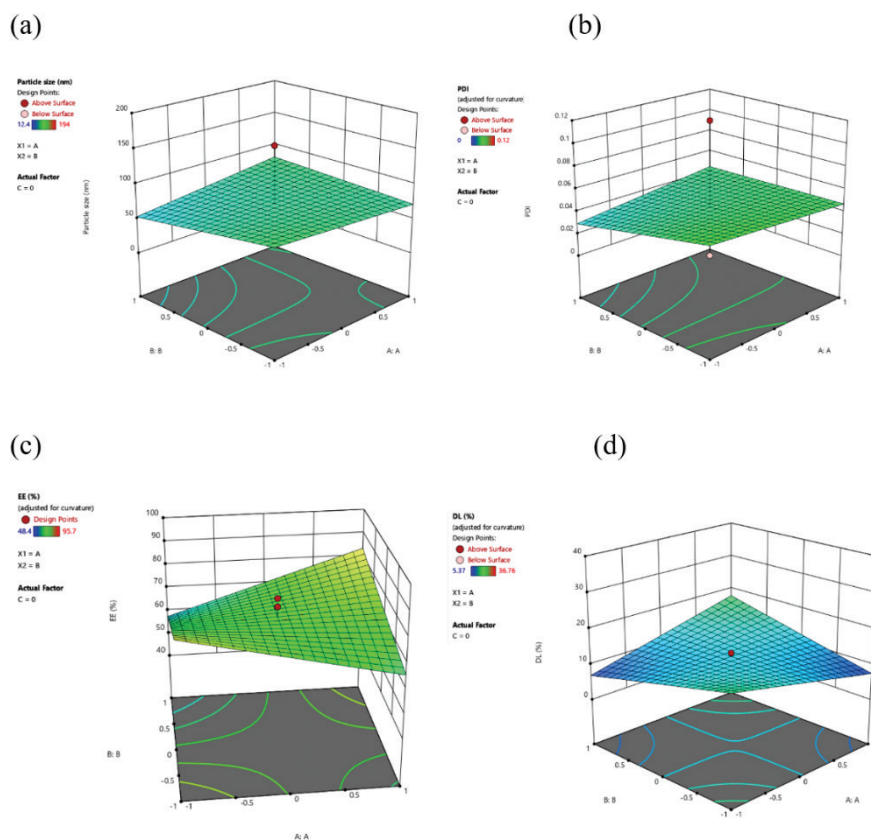


**Figure 3.** Response surface 3D plots showing the effect of independent variables on the dependent variables via (a) particle size, (b) PDI, (c) EE%, and (d) DL% by Design-Expert® software.

$$R_4 = 12.36 + 0.3181A + 0.0344B - 0.1606C + 5.14AB - 3.80AC - 3.77BC - 0.6944ABC \quad \text{E.q. 5}$$

The DL% ( $R_4$ ) analysis revealed that the coefficient has a positive sign for stabilisers A and B, while stabiliser C possesses a negative charge. The stabiliser possesses a negative charge on DL%, indicating that increasing stabiliser concentration would decrease DL%. The response surface 3D plots revealed that the DL% is heading toward the upper level at low stabiliser concentration, as shown in Fig. 3d.

## Optimisation and evaluation of the prepared formulations

Optimisation aims to find the variables that could dramatically affect the chosen responses and specify the level of variables that a high-quality and robust product might produce (Zidan et al. 2007). The measured responses affecting the product's quality should be considered during optimisation. The criteria of the responses were: particle size  $\leq 100$ , PDI  $\leq 0.1$ , EE%  $\geq 50$  and DL%  $\geq 10$ . Factorial formulation responses suggested 150 mg, 180 mg, and 82 mg of PVP K-30, HPMC E5 and PXM-188, respectively. The predicted particle size values were 72.56 nm, PDI was 0.049, EE% was 73.34% and DL% was 12.04%. The selected optimised formulation was prepared, and the observed values were found to be quite comparable to the predicted values. The experimental (found) particle size values were 64.65 nm, PDI was 0.059, EE% was 86.73% and DL% was 10.17%. Relative errors of experimental and predicted values are calculated in Equation 6.

$$\text{Relative error} = \frac{(\text{predicted} - \text{experimental})}{\text{predicted}} \quad \text{E.q. 6}$$

The relative error of particle size was 0.1, PDI was 0.2, EE% was 0.18, and DL% was 0.16, reflecting an agreement between predicted and experimental values. Results from this analysis demonstrate a model's ascertained viability (Rane et al. 2007).

## Morphological studies using AFM analysis

The morphological analysis and particle size of Candesartan cilexetil-loaded nanosuspensions performed by AFM show regular to spherical-shaped nanoparticles with a size of 30.4 nm and approved by the particle size distribution histogram, as shown in Fig. 4. In contrast, the ABT-9000 particle size analyser estimated the particle size was 64.65 nm. The particle size of the optimised Candesartan cilexetil-loaded nanosuspensions obtained by AFM was smaller than that measured by the ABT-9000 particle size analyser, and this difference was because a particle size analyser could only provide data on the volumetric mean diameter of a large number of particles; it is challenging to get findings that reflect actual size distribution.

## Drug-excipient compatibility studies using FTIR

Pure candesartan cilexetil revealed peaks at 2950.5  $\text{cm}^{-1}$  due to aromatic C-H stretching and 2870.2  $\text{cm}^{-1}$  due to O-H stretching, as shown in Fig. 5A. Peaks were revealed at 1752.13  $\text{cm}^{-1}$  and 1718.01  $\text{cm}^{-1}$  due to ester C=O stretching vibration, whereas peaks at 1271.12  $\text{cm}^{-1}$  and 1315.83  $\text{cm}^{-1}$  for C-O stretching of the carbonyl group of aromatic esters. Peaks were revealed at 1030–1281  $\text{cm}^{-1}$  for N-C stretching of the drug.

For PVP k30, there is a strong absorbance band at 1675.25  $\text{cm}^{-1}$  due to the C=O of tertiary amide and at 2358.17  $\text{cm}^{-1}$  due to C-H stretching. A vast band was shown at 3264.15  $\text{cm}^{-1}$  due to O-H stretching vibrations of absorbed water (Fig. 5B). The broadband was confirmed by DSC analysis as the broad endothermic peak. Results from these experiments were consistent with the findings of Wegiel and his colleagues (2014), who had similar FTIR peaks (Wegiel et al. 2014). HPMC E5 analysis showed a peak at 3312  $\text{cm}^{-1}$  due to O-H stretching vibration, 1170.13  $\text{cm}^{-1}$  due to C-O-C stretching vibration, and 1103.07  $\text{cm}^{-1}$  (Fig. 5C) due to C-O stretching. The findings from this analysis agreed with the findings of Oh and his colleagues (2012) (Oh et al. 2012). The FTIR spectrum of PXM 188 revealed a principal absorption peak at 3287.44  $\text{cm}^{-1}$  due to aliphatic C-H stretching (Fig. 5D). Also, the O-H bending appeared at 1344.03  $\text{cm}^{-1}$ , and C-O stretching at 1121  $\text{cm}^{-1}$ . Sharma and his colleagues (2013) have found the same results (Sharma et al. 2013).

The FTIR peaks of nanosuspensions-free candesartan cilexetil revealed peaks at 3435.22  $\text{cm}^{-1}$ , 2347.37  $\text{cm}^{-1}$ , 1645.26  $\text{cm}^{-1}$  and 1093.64  $\text{cm}^{-1}$  for PVP K-30 and HPMC E5 (O-H stretching), PXM 188 (O-H bending), PVP K-30 (C=O of tertiary amide) and HPMC E5 and PXM 188 (C-O stretching) (Fig. 5E). The C=O stretching vibration peak of candesartan cilexetil disappeared in the nanosuspensions complex of candesartan cilexetil/polymers (Fig. 5E). The candesartan cilexetil revealed a C=O stretching vibration peak, indicating an H-bonding between the drug and polymer, as shown in Fig. 5F. There was no significant shift in the FTIR spectrum, indicating no interaction or complexation between payload and polymers during the preparation of candesartan-cilexetil nanosuspensions. The characteristic peaks of the Candesartan cilexetil-loaded nanosuspensions in the region of 2870.2  $\text{cm}^{-1}$ –2950.5  $\text{cm}^{-1}$  were observed in the loaded nanosuspensions, revealing that the drug was entrapped physically inside the nanosuspensions.

## Compatibility analysis using DSC analysis

The thermal behaviour of candesartan cilexetil and polymers is depicted in Fig. 6A–F. The classic application of the DSC analysis is determining any possible interactions between the entity of a drug and its

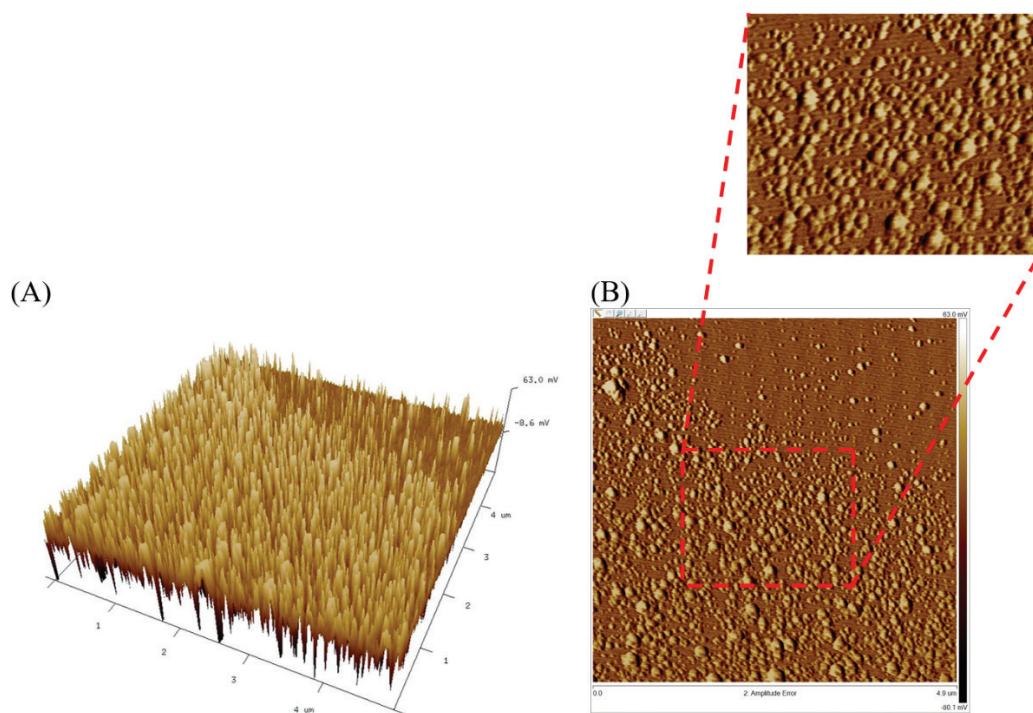


**Figure 4.** The AFM images of the Candesartan cilexetil-loaded nanosuspensions. **A.** 3D AFM image of candesartan cilexetil-loaded nanosuspensions; **B.** 2D AFM image of candesartan cilexetil-loaded nanosuspensions.

excipients within a formulation. The formation of candesartan cilexetil inclusion complexes and host-guest interactions lead to boiling, glass transition, melting, and sublimation points disappearing or shifting to different temperatures. The polymers' effect on the candesartan cilexetil's inner structure was investigated using DSC analysis.

The pure Candesartan cilexetil DSC curve revealed a sharp endothermic peak at 165 °C, corresponding to its melting followed by an exothermic peak, indicating its crystalline nature (Fig. 6A). This result was consistent with the results of Gurunath et al. (Gurunath et al. 2014). However, the endothermic peak of the candesartan cilexetil was shifted (towards lower temperature), slightly broadened and reduced in intensity in Candesartan cilexetil-loaded nanosuspensions (Fig. 6B). This behaviour could be due to the uniform distribution of the candesartan cilexetil in the polymer's crust, causing the molten drug's entire miscibility in polymers. Also, the DSC results revealed no interactions between the lipophilic excipients and the drug (Kamalakkannan et al. 2013). A broad endotherm peak was also realised at 55 °C due to the water.

The candesartan cilexetil-free nanosuspensions revealed a vast, broad endotherm peak at 140–170 °C (Fig. 6C). The DSC thermogram of PVP K30 polymer revealed a broad endotherm peak ranging from 20 to 90 °C due to its highly hygroscopic nature (Fig. 7D) (Sethia and Squillante 2004). An amorphous characteristic of PVP K30 polymer was suggested from the results above. A broad endothermic peak, ranging from 15 to 100 °C, was also seen in the DSC thermogram of HPMC E5 due to the pos-

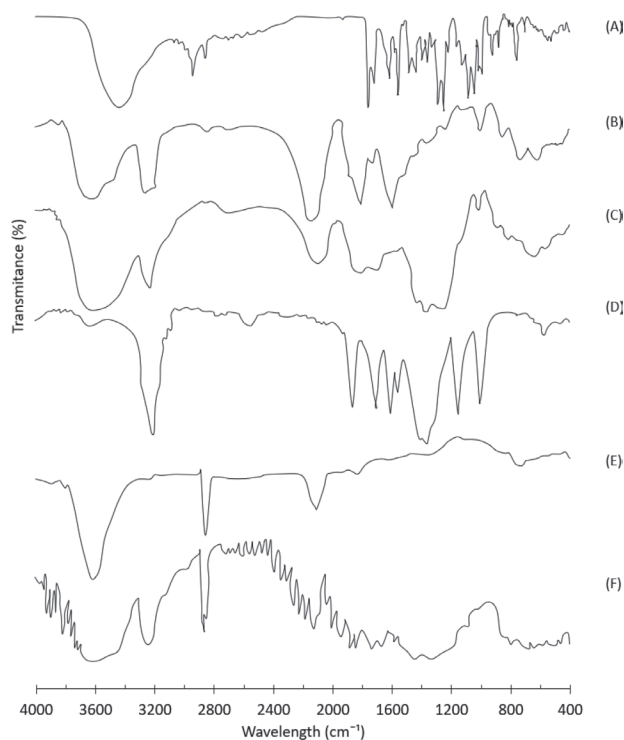


**Figure 5.** FTIR spectrum of **A.** Pure candesartan cilexetil compound; **B.** PVP K-30 polymer; **C.** HPMC E5 polymer; **D.** PXM 188 polymer; **E.** Candesartan cilexetil-free nanosuspensions; and **F.** Candesartan cilexetil-loaded nanosuspensions.

sible dehydration of water molecules (Zaini et al. 2017). The PXM 188 revealed an endothermic melting peak at 51.73 °C, as shown in Fig. 6F.

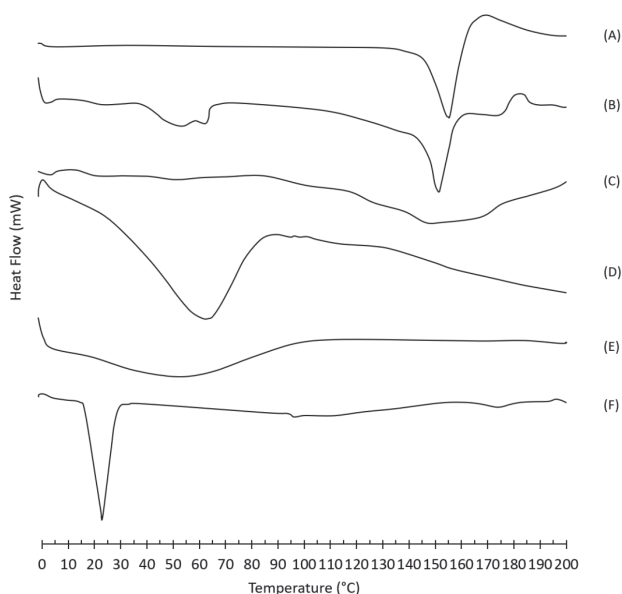


**Figure 6.** The DSC thermogram of **A.** pure candesartan cilexetil; **B.** Candesartan cilexetil-loaded nanosuspensions; **C.** Candesartan cilexetil-free nanosuspensions; **D.** PVP K-30; **E.** HPMS E5; **F.** PXM 188.

### In vitro release study

The dissolution rate of the payload has a significant effect on the absorption and, consequently, bioavailability. Therefore, comparing the dissolution profiles of different formulations is essential. The *in vitro* results of the following study for Candesartan cilexetil-loaded nanosuspensions and Candesartan cilexetil powder revealed > 95% release in PBS (pH 6.8) (Fig. 7A) and HCl buffer (pH 1.2) (Fig. 7B) within one hour with a steep profile. The release from candesartan cilexetil powder revealed 62% in PBS (pH 6.8) (Fig. 7A) and 36% in HCl buffer (pH 1.2) within one hour with the slow graduate profile. The *in vitro* release study revealed a significant ( $p$ -value  $\leq 0.05$ ) increase in the dissolution rate of the candesartan cilexetil. In general, the Candesartan cilexetil powder was released slowly in HCl buffer (pH 1.2) compared to PBS buffer (pH 6.8), which could result from the solubility difference of candesartan cilexetil in these media.

On the other hand, the release profile of Candesartan cilexetil-loaded nanosuspensions exhibited a biphasic pattern with an initial rapid phase followed by a slow phase in PBS and in HCl buffers. The fast release phase might be due to the burst release of the payload. A possible explanation is the enrichment of the payload in the nanosuspension's outer region. Thus, a short diffusion path would be carried out (zur Mühlen et al. 1998).

### Stability study

Stability studies included analysis of the particle size and EE % over three months at 32 °C, 25 °C and 4 °C. Analysis of particle size after three months at 32 °C, 25 °C and 4 °C was 75.5, 69.3 and 66.4 nm, respectively, as shown in Fig. 8A. No significant differences ( $P \leq 0.5$ ) in nanosuspension

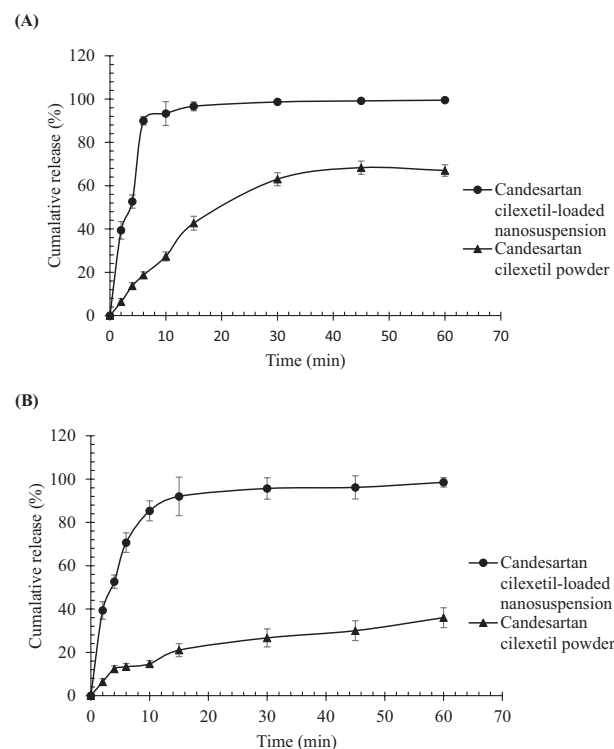


**Figure 7.** The *in vitro* release profile of Candesartan cilexetil-loaded nanosuspensions and Candesartan cilexetil powder at **A.** Dissolution medium phosphate buffer (pH 6.8) and **B.** Dissolution medium HCl buffer (pH 1.2). Data are represented as mean  $\pm$  standard deviation of three independent experiments.

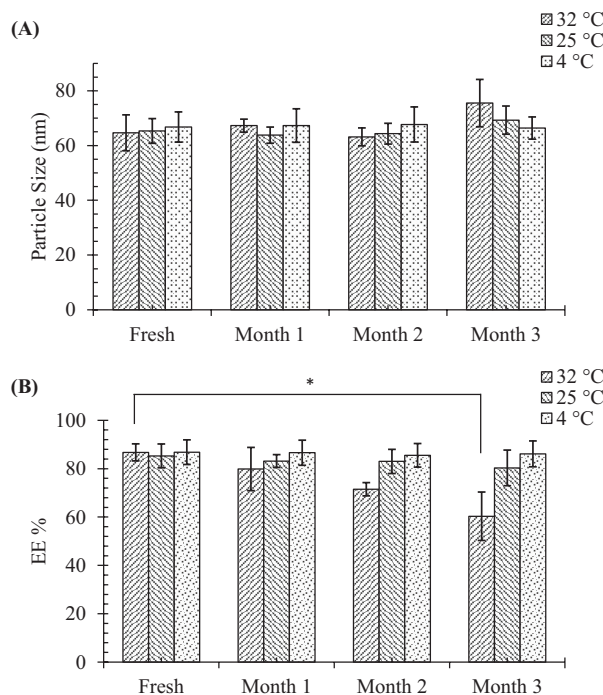


**Figure 8.** Particle size and EE % analysis of the Candesartan cilexetil-loaded nanosuspensions. **A.** Particle size and **B.** EE % over three months at 32 °C, 25 °C and 4 °C. Data are represented as mean  $\pm$  standard deviation of three independent experiments. \*  $p$ -value > 0.05.

particle sizes reflected a stable formulation over the studied period. On the other hand, the EE % of the Candesartan cilexetil after three months at 32 °C, 25 °C, and 4 °C was 60, 80, and 86, respectively, as shown in Fig. 8B. There was a significant difference ( $p > 0.05$ ) in the EE % of the candesartan cilexetil at 32 °C, reflecting the inability to stand the same concentration at this temperature. However, no significant differences ( $P \leq 0.5$ ) were found at 25 °C and 4 °C.

## Conclusions

The formulation strategy of using nanosuspensions was investigated as an effective way to improve the solubility of candesartan cilexetil. The solvent evaporation

technique, with the aid of Design-Expert® software, was effective in producing a stable preparation and nanosizing the drug. This study accomplished the particle size of 64.65 nm with a narrow PDI (0.059) and a good E.E. % of 86.75%. The solubility of candesartan cilexetil was enhanced five-fold more than bulk powder by loading it into nanosuspensions. The AFM results revealed nanosuspensions exhibiting a smooth surface and spherical particles. The FTIR and DSC results confirmed the unchanged crystalline nature of candesartan cilexetil in the candesartan cilexetil-loaded nanosuspension. The *in vitro* dissolution profile revealed a 30% increase in the dissolution rate compared to the drug powder. Stability studied over three months showed stable Candesartan cilexetil-loaded nanosuspension with no significant changes in particle sizes and EE %.

## References

- Abbas HK, Wais FMH, Abood AN (2017) Preparation and evaluation of ketoprofen nanosuspension using solvent evaporation technique. *Iraqi Journal of Pharmaceutical Sciences* 26(2): 41–55. <https://doi.org/10.31351/vol26iss2pp41-55>
- Abdalla KF, Kamoun EA, El Maghraby GM (2015) Optimization of the entrapment efficiency and release of ambroxol hydrochloride alginate beads. *Journal of Applied Pharmaceutical Science* 5: 13–19. <https://doi.org/10.7324/JAPS.2015.50403>
- Adeli H, Khorasani MT, Parvazinia M (2019) Wound dressing based on electrospun PVA/chitosan/starch nanofibrous mats: Fabrication, antibacterial and cytocompatibility evaluation and *in vitro* healing assay. *International Journal of Biological Macromolecules* 122: 238–254. <https://doi.org/10.1016/j.ijbiomac.2018.10.115>
- Ahmed TA, Aljaeid BM (2017) A potential *in situ* gel formulation loaded with novel fabricated poly (lactide-co-glycolide) nanoparticles for enhancing and sustaining the ophthalmic delivery of ketoconazole. *International Journal of Nanomedicine* 12: 1863–1875. <https://doi.org/10.2147/IJN.S131850>
- Al-Edresi S, Alsalahat I, Freeman S, Aojula H, Penny J (2020) Resveratrol-mediated cleavage of amyloid  $\beta(1-42)$  peptide: potential relevance to Alzheimer's disease. *Neurobiol Aging* 94: 24–33. <https://doi.org/10.1016/j.neurobiolaging.2020.04.012>
- Al-Shaibani AJN, Al-Gburi KMH, Albo Hamraha KTK, Abd Alridha AM (2019) Design and characterization of candesartan cilexetil oral nanoemulsion containing garlic oil. *International Journal of Applied Pharmaceutics* 11: 116–124. <https://doi.org/10.22159/ijap.2019v11i6.35066>
- Albo Hamrah KTK, Al-Shaibani AJN, Al-Edresi SS, Al-Gburi KMH (2020) A comparative study of quality control testing on candesartan cilexetil conventional tablets in Iraq. *International Journal of Applied Pharmaceutics* 12: 103–108. <https://doi.org/10.22159/ijap.2020v12i2.36220>
- Aledresi SS, Abdulrazzaq IF, Alshaibani AJ (2020) Enhancing the solubility of nimesulide by loading to a nanoemulsion. *Latin American Journal of Pharmacy* 39: 2299–2308.
- Alhagiesha AW, Ghareeb MM (2021) The formulation and characterization of nimodipine nanoparticles for the enhancement of solubility and dissolution rate. *Iraqi Journal of Pharmaceutical Sciences* 30: 143–152. <https://doi.org/10.31351/vol30iss2pp143-152>
- Aly UF, Sarhan HA, Ali TFS, Sharkawy HAE (2020) Applying different techniques to improve the bioavailability of candesartan cilexetil antihypertensive drug. *Drug Design, Development and Therapy* 14: 1851–1865. <https://doi.org/10.2147/DDDT.S248511>
- Archana D, Singh BK, Dutta J, Dutta PK (2015) Chitosan-PVP-nano silver oxide wound dressing: In vitro and in vivo evaluation. *International Journal of Biological Macromolecules* 73: 49–57. <https://doi.org/10.1016/j.ijbiomac.2014.10.055>
- Ardiana F, Lestari MLAD, Indrayanto G (2012) Chapter 3 - Candesartan Cilexetil. In: Brittain Harry G (Ed.) *Profiles of Drug Substances, Excipients and Related Methodology*. Academic Press, 79–112. <https://doi.org/10.1016/B978-0-12-397220-0.00003-9>
- Aydogdu A, Yildiz E, Ayhan Z, Aydogdu Y, Sumnu G, Sahin SJEPEJ (2019) Nanostructured poly (lactic acid)/soy protein/HPMC films by electrospinning for potential applications in food industry. *European Polymer Journal* 112: 477–486. <https://doi.org/10.1016/j.eurpolymj.2019.01.006>
- Balogh A, Farkas B, Verreck G, Mensch J, Borbás E, Nagy B, Marosi G, Nagy ZK (2016) AC and DC electrospinning of hydroxypropylmethylcellulose with polyethylene oxides as secondary polymer for improved drug dissolution. *International Journal of Pharmaceutics* 505: 159–166. <https://doi.org/10.1016/j.ijpharm.2016.03.024>
- Bhakay A, Rahman M, Dave RN, Bilgili E (2018) Bioavailability enhancement of poorly water-soluble drugs *via* nanocomposites: Formulation–Processing aspects and challenges. *Pharmaceutics* 10: 1–62. <https://doi.org/10.3390/pharmaceutics10030086>
- Bonthagarala B, Sai P, Venkata S (2015) Enhancement of dissolution rate of clofibrate (BCS Class–II drug) by using liquisolid compact technology. *International Journal of Biomedical and Advance Research* 6: 288–298. <https://doi.org/10.7439/ijbar.v6i3.1891>
- Chen L, Wang Y, Zhang J, Hao L, Guo H, Lou H, Zhang D (2014) Bexarotene nanocrystal-oral and parenteral formulation development, characterization and pharmacokinetic evaluation. *European Journal of Pharmaceutics and Biopharmaceutics* 87: 160–169. <https://doi.org/10.1016/j.ejpb.2013.12.005>
- Dabhi MR, Ghodasara UK, Mori DD, Patel KA, Manek R, Sheth NR (2015) Formulation, optimization and characterization of candesartan cilexetil nanosuspension for *in vitro* dissolution enhancement.

- African Journal of Pharmacy and Pharmacology 9: 102–113. <https://doi.org/10.5897/AJPP2013.3887>
- Demirci S, Alaslan A, Caykara T (2009) Preparation, characterization and surface pKa values of poly(N-vinyl-2-pyrrolidone)/chitosan blend films. *Applied Surface Science* 255: 5979–5983. <https://doi.org/10.1016/j.apsusc.2009.01.050>
- Detroja C, Chavhan S, Sawant K (2011) Enhanced antihypertensive activity of candesartan cilexetil nanosuspension: formulation, characterization and pharmacodynamic study. *Scientia Pharmaceutica* 79: 635–651. <https://doi.org/10.3797/scipharm.1103-17>
- Dolenc A, Govedarica B, Kocbek P, Srčić S, Kristl J (2010) Nanosized particles of orlistat with enhanced *in vitro* dissolution rate and lipase inhibition. *International Journal of Pharmaceutics* 396: 149–155. <https://doi.org/10.1016/j.ijpharm.2010.06.003>
- Dora CP, Singh SK, Kumar S, Datusalia AK, Deep A (2010) Development and characterization of nanoparticles of glibenclamide by solvent displacement method. *Acta Poloniae Pharmaceutica* 67: 283–290.
- Edis Z, Wang J, Waqas MK, Ijaz M, Ijaz M (2021) Nanocarriers-mediated drug delivery systems for anticancer agents: An overview and perspectives. *International Journal of Nanomedicine* 16: 1313–1330. <https://doi.org/10.2147/IJN.S289443>
- Figuroa-Campos A, Sánchez-Dengra B, Merino V, Dahan A, González-Álvarez I, García-Arieta A, González-Álvarez M, Bermejo M (2020) Candesartan Cilexetil In Vitro-In Vivo Correlation: Predictive Dissolution as a Development Tool. *Pharmaceutics* 12(7): 633. <https://doi.org/10.3390/pharmaceutics12070633>
- Fonte P, Reis S, Sarmiento B (2016) Facts and evidences on the lyophilization of polymeric nanoparticles for drug delivery. *Journal of Controlled Release* 225: 75–86. <https://doi.org/10.1016/j.jconrel.2016.01.034>
- Gadad A, Dandagi P, Mastiholimath V (2012) Moxifloxacin loaded polymeric nanoparticles for sustained ocular drug delivery. *International Journal of Pharmaceutical Sciences and Nanotechnology* 5: 1727–1734. <https://doi.org/10.37285/ijpsn.2012.5.2.8>
- Gigliobianco MR, Casadidio C, Censi R, Di Martino P (2018) Nanocrystals of Poorly Soluble Drugs: Drug Bioavailability and Physicochemical Stability. *Pharmaceutics* 10: 134. <https://doi.org/10.3390/pharmaceutics10030134>
- Gurunath S, Nanjwade BK, Patila PA (2014) Enhanced solubility and intestinal absorption of candesartan cilexetil solid dispersions using everted rat intestinal sacs. *Saudi Pharmaceutical Journal* 22: 246–257. <https://doi.org/10.1016/j.jsps.2013.03.006>
- Hao Y-M (2011) Entrapment and release difference resulting from hydrogen bonding interactions in niosome. *International Journal of Pharmaceutics* 403: 245–253. <https://doi.org/10.1016/j.ijpharm.2010.10.027>
- Hoppe K, Sznitowska M (2014) The effect of polysorbate 20 on solubility and stability of candesartan cilexetil in dissolution media. *AAPS PharmSci-Tech* 15: 1116–1125. <https://doi.org/10.1208/s12249-014-0109-8>
- Huang T, Wang Y, Shen Y, Ao H, Guo Y, Han M, Wang X (2020) Preparation of high drug-loading celastrol nanosuspensions and their anti-breast cancer activities *in vitro* and *in vivo*. *Scientific Reports* 10: 1–9. <https://doi.org/10.1038/s41598-020-65773-9>
- Isailović BD, Kostić IT, Zvonar A, Đorđević VB, Gašperlin M, Nedović VA, Bugarski BM (2013) Resveratrol loaded liposomes produced by different techniques. *Innovative Food Science & Emerging Technologies* 19: 181–189. <https://doi.org/10.1016/j.ifset.2013.03.006>
- Jacob S, Nair AB (2018) Cyclodextrin complexes: Perspective from drug delivery and formulation. *Drug Development Research* 79: 201–217. <https://doi.org/10.1002/ddr.21452>
- Jassim ZE, Hussein AA (2014) Formulation and evaluation of clopidogrel tablet incorporating drug nanoparticles. *International Journal of Pharmacy and Pharmaceutical Sciences* 6: 838–851.
- Jia L, Wong H, Cerna C, Weitman SD (2002) Effect of nanonization on absorption of 301029: ex vivo and in vivo pharmacokinetic correlations determined by liquid chromatography/mass spectrometry. *Pharmaceutical Research* 19: 1091–1096. <https://doi.org/10.1023/A:1019829622088>
- Kamalakkannan V, Puratchikody A, Ramanathan L (2013) Development and characterization of controlled release polar lipid microparticles of candesartan cilexetil by solid dispersion. *Research in Pharmaceutical Sciences* 8: 125–136.
- Kumar M, Jha A, Dr M, Mishra B (2020) Targeted drug nanocrystals for pulmonary delivery: A potential strategy for lung cancer therapy. *Expert Opinion on Drug Delivery* 17: 1459–1472. <https://doi.org/10.1080/17425247.2020.1798401>
- Li G, Lu Y, Fan Y, Ning Q, Li W (2020) Enhanced oral bioavailability of magnolol via mixed micelles and nanosuspensions based on Soluplus®-Poloxamer 188. *Drug Delivery* 27: 1010–1017. <https://doi.org/10.1080/10717544.2020.1785582>
- Liu P, Viitala T, Kartal-Hodzic A, Liang H, Laaksonen T, Hirvonen J, Peltonen L (2015) Interaction studies between indomethacin nanocrystals and PEO/PPO copolymer stabilizers. *Pharmaceutical Research* 32: 628–639. <https://doi.org/10.1007/s11095-014-1491-3>
- Madan JR, Adokar BR, Dua K (2015) Development and evaluation of *in situ* gel of pregabalin. *International Journal of Pharmaceutical Investigation* 5: 226–233. <https://doi.org/10.4103/2230-973X.167686>
- Mandlik SK, Ranpise NS (2017) Implementation of experimental design methodology in preparation and characterization of zolmitriptan loaded chitosan nanoparticles. *International Journal of Current Pharmaceutical Research* 6: 16–22. <https://doi.org/10.3329/icpj.v6i3.32684>
- Mittal S, Chaudhary A, Chaudhary A, Kumar A (2020) Proniosomes: the effective and efficient drug-carrier system. *Therapeutic Delivery* 11: 125–137. <https://doi.org/10.4155/tde-2019-0065>
- Müller RH, Jacobs C, Kayser O (2001) Nanosuspensions as particulate drug formulations in therapy. Rationale for development and what we can expect for the future. *Advanced Drug Delivery Reviews* 47: 3–19. [https://doi.org/10.1016/S0169-409X\(00\)00118-6](https://doi.org/10.1016/S0169-409X(00)00118-6)
- Oh MJ, Shim JB, Yoo H, Lee GY, Jo H, Jeong SM, Yuk SH, Lee D, Khang G (2012) The dissolution property of raloxifene HCl solid dispersion using hydroxypropyl methylcellulose. *Macromolecular Research* 20: 835–841. <https://doi.org/10.1007/s13233-012-0127-x>
- Powar T, Hajare A (2020) Lyophilized ethinylestradiol nanosuspension: fabrication, characterization and evaluation of *in vitro* anticancer and pharmacokinetic study. *Indian Journal of Pharmaceutical Sciences* 82: 54–59. <https://doi.org/10.36468/pharmaceutical-sciences.622>
- Pradhan KK, Mishra US, Pattnaik S, Panda CK, Sahu KC (2011) Development and Validation of a Stability-indicating UV Spectroscopic Method for Candesartan in Bulk and Formulations. *Indian Journal of Pharmaceutical Sciences* 73: 693–696. <https://doi.org/10.4103/0250-474X.100254>
- Rane Y, Mashru R, Sankalia M, Sankalia J (2007) Effect of hydrophilic swellable polymers on dissolution enhancement of carbamazepine

- solid dispersions studied using response surface methodology. *AAPS PharmSciTech* 8: E1–E11. <https://doi.org/10.1208/pt0802027>
- Rizal S, Abdullah C, Olaiya N, Sri Aprilia N, Zein I, Surya I, Abdul Khalil H (2020) Preparation of palm oil ash nanoparticles: Taguchi optimization method by particle size distribution and morphological studies. *Applied Sciences* 10: 1–15. <https://doi.org/10.3390/app10030985>
- Sahu B, Das M (2013) Optimization of felodipine nanosuspensions using full factorial design. *International Journal of PharmTech Research* 5: 553–561.
- Sambhakar S, Paliwal S, Sharma S, Singh B (2017) Formulation of risperidone loaded proniosomes for effective transdermal delivery: An in-vitro and in-vivo study. *Bulletin of Faculty of Pharmacy, Cairo University* 55: 239–247. <https://doi.org/10.1016/j.bfopcu.2017.09.003>
- Satyajit C, Rao MB, Patro CN, Swain S, Taria S, Kumar S (2014) Formulation, characterization and *in vitro* evaluation for solubility enhancement of a poorly water soluble drug using nanoedge technique. *World Journal of Pharmaceutical Research* 3: 2152–2167.
- Sethia S, Squillante E (2004) Solid dispersion of carbamazepine in PVP K30 by conventional solvent evaporation and supercritical methods. *International Journal of Pharmaceutics* 272: 1–10. <https://doi.org/10.1016/j.ijpharm.2003.11.025>
- Shah J, Nair AB, Shah H, Jacob S, Shehata TM, Morsy MA (2020) Enhancement in antinociceptive and anti-inflammatory effects of tramadol by transdermal proniosome gel. *Asian Journal of Pharmaceutical Sciences* 15: 786–796. <https://doi.org/10.1016/j.ajps.2019.05.001>
- Sharma A, Jain CP, Tanwar YS (2013) Preparation and characterization of solid dispersions of carvedilol with poloxamer 188. *Journal of the Chilean Chemical Society* 58: 1553–1557. <https://doi.org/10.4067/S0717-97072013000100012>
- Sharma M, Kohli S, Dinda A (2015) *In vitro* and *in vivo* evaluation of repaglinide loaded floating microspheres prepared from different viscosity grades of HPMC polymer. *Saudi Pharmaceutical Journal* 23: 675–682. <https://doi.org/10.1016/j.jsps.2015.02.013>
- Tadros TF (2017) 7. Ostwald ripening in suspensions. In: *Suspension Concentrates*. De Gruyter, Berlin, Boston, 137–152. <https://doi.org/10.1515/9783110486872-008>
- Van Eerdenbrugh B, Vermant J, Martens JA, Froyen L, Van Humbeek J, Augustijns P, Van den Mooter G (2009) A screening study of surface stabilization during the production of drug nanocrystals. *Journal of Pharmaceutical Sciences* 98: 2091–2103. <https://doi.org/10.1002/jps.21563>
- Wang B-l, Wang J-l, Li D-d, Ren K-f, Ji J (2012) Chitosan/poly (vinyl pyrrolidone) coatings improve the antibacterial properties of poly(ethylene terephthalate). *Applied Surface Science* 258: 7801–7808. <https://doi.org/10.1016/j.apsusc.2012.03.181>
- Wegiel LA, Mauer LJ, Edgar KJ, Taylor LS (2014) Mid-infrared spectroscopy as a polymer selection tool for formulating amorphous solid dispersions. *Journal of Pharmacy and Pharmacology* 66: 244–255. <https://doi.org/10.1111/jphp.12079>
- Wilk S, Benko A (2021) Advances in fabricating the electrospun biopolymer-based biomaterials. *Journal of Functional Biomaterials* 12: 1–32. <https://doi.org/10.3390/jfb12020026>
- Zaini E, Fitriani L, Effendy S, Noviza D, Halim A (2017) Preparation and characterization of solid dispersion telmisartan–hydroxypropyl methyl cellulose (HPMC) E5 LV by co-grinding method. *Oriental Journal of Chemistry* 33: 873–878. <https://doi.org/10.13005/ojc/330236>
- Zhang W, Wang G, See E, Shaw JP, Baguley BC, Liu J, Amirapu S, Wu Z (2015) Post-insertion of poloxamer 188 strengthened liposomal membrane and reduced drug irritancy and *in vivo* precipitation, superior to PEGylation. *Journal of Controlled Release* 203: 161–169. <https://doi.org/10.1016/j.jconrel.2015.02.026>
- Zidan AS, Sammour OA, Hammad MA, Megrab NA, Habib MJ, Khan MA (2007) Quality by design: understanding the formulation variables of a cyclosporine A self-nanoemulsified drug delivery systems by Box-Behnken design and desirability function. *International Journal of Pharmaceutics* 332: 55–63. <https://doi.org/10.1016/j.ijpharm.2006.09.060>
- zur Mühlen A, Schwarz C, Mehnert W (1998) Solid lipid nanoparticles (SLN) for controlled drug delivery--drug release and release mechanism. *European Journal of Pharmaceutics and Biopharmaceutics* 45: 149–155. [https://doi.org/10.1016/S0939-6411\(97\)00150-1](https://doi.org/10.1016/S0939-6411(97)00150-1)